IEEE Access
Multidisciplinary | Rapid Review | Open Access Journal

Received February 10, 2019, accepted March 27, 2019, date of publication April 1, 2019, date of current version April 15, 2019.

Digital Object Identifier 10.1109/ACCESS.2019.2908719

Relationship Between the Nonlinear Oscillator and the Motor Cortex

QIANG LU
College of Medical Information Engineering, Shandong First Medical University & Shandong Academy of Medical Sciences, Tai'an 271016, China
luqiang271016@163.com

This work was supported in part by the Shandong Provincial Natural Science Foundation, China, under Grant ZR2017MF039, and in part by the Project of Shandong Province Higher Educational Science and Technology Program, China, under Grant J18KA358.

ABSTRACT The investigations show that the fractional calculus could be employed for complex biological systems and capture intrinsic phenomena. At the same time, the research results also show that the neural network has the characteristics of fractional calculus and its neuronal dynamics is complex. As a micro-neural circuit placed in the spinal cord, the central pattern generator (CPG) is supposed to have the property of fractional calculus. In order to study the application of the fractional order technique to the CPG, the fractional order CPG model is established based on the Matsuoka model. The stable conditions are given through mathematical analysis. In order to extract the relation between the motor cortex and the fractional order CPG, the coupling model between the fractional order CPG and the neural mass model (NMM) simulated the motor cortex is built. Moreover, the effects of coupling model parameters variations on the CPG and the NMM are investigated. The main findings are: first, the CPG output obtained with the fractional order is more accurate than the one obtained with the integral order. Increasing the fractional order makes the CPG output more accurate. Second, the results show that the motor cortex has corresponding modes with those of the CPG. And the NMM mode can switch in accordance with the change of fractional order. Third, the simulations also show that a new stable state in motor cortex could be produced based on the existing modes with the introduction of the fractional order CPG model. It can provide a helpful method to understand the working principles of the motor cortex.

INDEX TERMS Central pattern generator, neural mass model, fractional calculus, motor cortex, limit cycle.

I. INTRODUCTION

The CPG consists of micro-neural circuits placed in spinal cord. It can generate rhythmic motor activity without descending and sensory inputs [1]–[3]. Previous works show that the CPG is found in vertebrates and invertebrates and its function is mainly for the motion of animals, such as walking and swimming [1], [2]. According to the working mechanism of the CPG, many mathematical CPG models are established and used in the locomotion control, such as Matsuoka model [4], [5], Wilson-Cowan neural model [6], Hopf oscillator [7] and Rayleigh oscillator [8]. In these CPG models, the state equations are usually integral order. There is no mathematical model with fractional calculus.

The fractional calculus extends ordinary differentiation and integration to their corresponding operations with arbitrary orders. The fractional calculus extend the concepts of differentiability and incorporate non-local and system memory effects through fractional order space and time derivatives. These characteristics allow researchers to model complex system using multiple time and space scales without dividing the problem into many smaller compartments. The extension of linear system model to fractional order model requires a new mathematical tool with which there are substantial issues associated with identifying the appropriate initial conditions and in selecting the proper definition of fractional integration for a given problem [9], [10]. Recently, many researchers have investigated the fractional calculus in different areas of physics and engineering [10]–[12]. Moaddy *et al.* [11] derived the fractional order cable model of the neuron system. Weinberg [12] employed a fractional order Hodgkin-Huxley neural model to describe the spiking features of the neuronal membrane patch, nerve axon, and the neural network. These investigations [10]–[13] show that the neural network has the character of fractional calculus and its neuronal dynamics is complex. The research results also show that the CPG is composed of different interneurons in which the typical ones are Shox2 [14] and Hb9 [15]. As a

The associate editor coordinating the review of this manuscript and approving it for publication was Victor Sanchez.

neural network, the CPG should have the property of fractional calculus. At the same time, the classical integral order CPG models [4]–[8] generate only smooth and fixed signal shapes. The features of the integral order CPG cannot explain the biological data [15]–[17] which have rich shapes and complex dynamics. Therefore, the fractional order CPG model is deserved to study. Since Matsuoka [4], [5] established the CPG model, the Matsuoka CPG has been widely applied to robot control [18], modeling [19] and made great progress because the CPG has many outstanding properties [4], [5]. In the paper, the fractional order CPG model is established based on the Matsuoka model [4], [5].

The locomotor network of non-mammalian vertebrates has been investigated in detailed, such as lamprey and the tadpoles [20], [21]. The investigations show that the motor cortex is coupled with the CPG [3] and the researchers confirm that the locomotion control system includes the motor cortex, CPG and the musculoskeletal system [3], [22]–[24]. However, the coupling relationship of the locomotor network for mammalians including human is still an open problem. Neural processes could generate the locomotor patterns. The basic rhythms and patterns of motoneuron activation could be controlled by the CPG during locomotion [24]. The sensory feedback from the moving limb influences each generator. The locomotor command regions are employed to activate these generators [3]. Therefore, the relationship among them should be investigated. The mathematical model and the computer simulation are effective tools to investigate this scientific problem. Murphy *et al.* [25] utilized a simplified musculoskeletal network model to simulate the organization of control modules in motor cortex. Kerkman *et al.* [26] used network analysis to investigate the relationship between anatomical and functional connectivity. The relation between the neural network and the integer order CPG was studied in the literature [19], [27], [28]. In this paper, the coupling model between the fractional order CPG and the motor cortex is built and the relationship is discussed.

The remainder of this paper is organized as follows. Section II studies the fractional order CPG model and its stability conditions. An appropriate coupling relation between the motor cortex and the fractional order CPG is also established in Section II. The effect of parameters variations on the motor cortex and the fractional order CPG is verified in Section III. Section IV gives some concluding remarks and future perspectives.

II. MODELS

A. THE FRACTIONAL ORDER CPG MODEL

The CPG model [4], [5], [19] is given by.

$$\begin{cases} T_r \dot{x}_1 + x_1 = -bx_2 - wg(x_3) + c \\ T_a \dot{x}_2 + x_2 = g(x_1) \\ T_r \dot{x}_3 + x_3 = -bx_4 - wg(x_1) + c \\ T_a \dot{x}_4 + x_4 = g(x_3) \end{cases} \tag{1}$$

where $g(\bullet)$ is a piecewise linear function describing the neurons threshold property. This function could be defined as $g(x) = \max(0, x)$. x_1 and x_3 represent the membrane potential. The adaptation and fatigue specification of the real neurons are described with two variables x_2 and x_4. The continuous adaptation of the tonic input during the stimulation procedure is described with adaptation parameter c. This adaptation during the stimulation process leads to action potentials. The mutual strength and self-inhibition are denoted by w and b, respectively. The time constants of x_1, x_3 and x_2, x_4 (that shows their reaction times) are denoted by T_r and T_a, respectively.

In order to analysis the equilibrium and stability of the model, the parameters T_r and T_a are set as 0.1 and 1, respectively. c is 0. Based on the method proposed in [4], (1) is linearized and the following simplified equation is obtained.

$$\begin{cases} \dot{x}_1 = 10(-x_1 - bx_2 - wx_3) \\ \dot{x}_2 = -x_2 + x_1 \\ \dot{x}_3 = 10(-x_3 - bx_4 - wx_1) \\ \dot{x}_4 = -x_4 + x_3 \end{cases} \tag{2}$$

According to the proposed method in [29], the fractional order differential equation of the CPG is obtained and shown below.

$$\begin{cases} D^\alpha x_1 = 10(-x_1 - bx_2 - wx_3) \\ D^\alpha x_2 = -x_2 + x_1 \\ D^\alpha x_3 = 10(-x_3 - bx_4 - wx_1) \\ D^\alpha x_4 = -x_4 + x_3 \end{cases} \tag{3}$$

where α is the order of fractional derivative and $0 < \alpha \leq 1$.

Then the equilibrium and stability of the fractional order equation are investigated.

Let $D^\alpha x_i (i = 1, ldots, 4) = 0$, (3) is changed to

$$\begin{cases} x_1 + bx_2 + wx_3 = 0 \\ x_1 = x_2 \\ x_3 + bx_4 + wx_1 = 0 \\ x_3 = x_4 \end{cases} \tag{4}$$

Therefore, the equilibrium is $x_i (i = 1, ldots, 4) = 0$ if $b + w \neq -1$ and $b - w \neq -1$.

Then, the Jacobian matrix of system (3) is obtained and shown below.

$$\begin{bmatrix} -10 & -10b & -10w & 0 \\ 1 & -1 & 0 & 0 \\ -10w & 0 & -10 & -10b \\ 0 & 0 & 1 & -1 \end{bmatrix} \tag{5}$$

The characteristic equation is

$$\lambda^2 + (11 + 10w)\lambda + 10(1 + b + w) = 0 \tag{6}$$

Or

$$\lambda^2 + (11 - 10w)\lambda + 10(1 + b - w) = 0 \tag{7}$$

The eigenvalues of (6) are

$$\lambda_{1,2} = \frac{-(11+10w) \pm \sqrt{(11+10w)^2 - 40(1+b+w)}}{2} \quad (8)$$

Based on the stability theorem [30], the system is asymptotically stable when $|\arg(\lambda)| \geq \alpha\pi/2$. Then I study the stability conditions of system (3) when α is 1.

(1) According to (8), the eigenvalues are real if: (a) $b \leq 0$. (b) $w \in (-\infty, -0.9 - 0.2\sqrt{10b}]$ or $w \in [-0.9 + 0.2\sqrt{10b}, +\infty)$ if $b > 0$. For positive sign before radical and $w > -1 - b$, $|\arg(\lambda)| = \pi$ that demonstrates the stability of system (3) while for the negative sign and $w > -1.1$, $|\arg(\lambda)| = \pi$ is obtained which confirms the stability of system (3), too.

(2) if $b > 0$, (8) has complex roots for $w \in (-0.9 - 0.2\sqrt{10b}, -0.9 + 0.2\sqrt{10b})$. For positive sign before the radical and $w > -1.1$, I have $|\arg(\lambda)| > \pi/2$. This leads to stability of system (3). For the negative sign case, it is obvious that $|\arg(\lambda)| > \pi/2$ which ensures the system stability.

The eigenvalues of (7) are

$$\lambda_{3,4} = \frac{-(11-10w) \pm \sqrt{(11-10w)^2 - 40(1+b-w)}}{2} \quad (9)$$

(1) Equation (9) has real roots for (a) $b \leq 0$. (b) ($w \in (-\infty, 0.9 - 0.2\sqrt{10b}]$ or $w \in [0.9 + 0.2\sqrt{10b}, +\infty)$) and $b > 0$. For positive sign before radical and $w < 1 + b$, $|\arg(\lambda)| = \pi$ is obtained that confirms the stability of system (3). Moreover, for the negative sign and $w < 1.1$, $|\arg(\lambda)| = \pi$ which proves the system (3) stability.

(2) If $b > 0$, (9) has two complex roots for $w \in (0.9 - 0.2\sqrt{10b}, 0.9 + 0.2\sqrt{10b})$. Positive sign before radical and $w < 1.1$ yield $|\arg(\lambda)| > \pi/2$ that confirms the stability of (3). Considering negative sign before radical gives $|\arg(\lambda)| > \pi/2$ or accordingly demonstrates the stability of system (3).

Then the simulation of the fractional order CPG model is studied. In the simulation, the fractional derivative definition of Grunwald-Letnikov (G-L) [10] is employed to calculate the output of the fractional order CPG model. The G-L definition of fractional derivative is shown below.

$${}^{GL}D^{\alpha}f(t) = \lim_{h\to 0} \frac{1}{h^{\alpha}} \sum_{i=0}^{(t-m)/h} (-1)^i \binom{\alpha}{i} f(t-ih) \quad (10)$$

where

$$\binom{\alpha}{i} = \frac{\Gamma(\alpha+1)}{\Gamma(i+1)\Gamma(\alpha-i+1)} \quad (11)$$

${}^{GL}D^{\alpha}$ is the fractional differential operator based on G-L definition. $f(t)$ is an arbitrary differentiable function. α is a non-integer number representing the fractional order. $[m, t]$ is the domain of $f(t)$. Γ is the Gamma function.

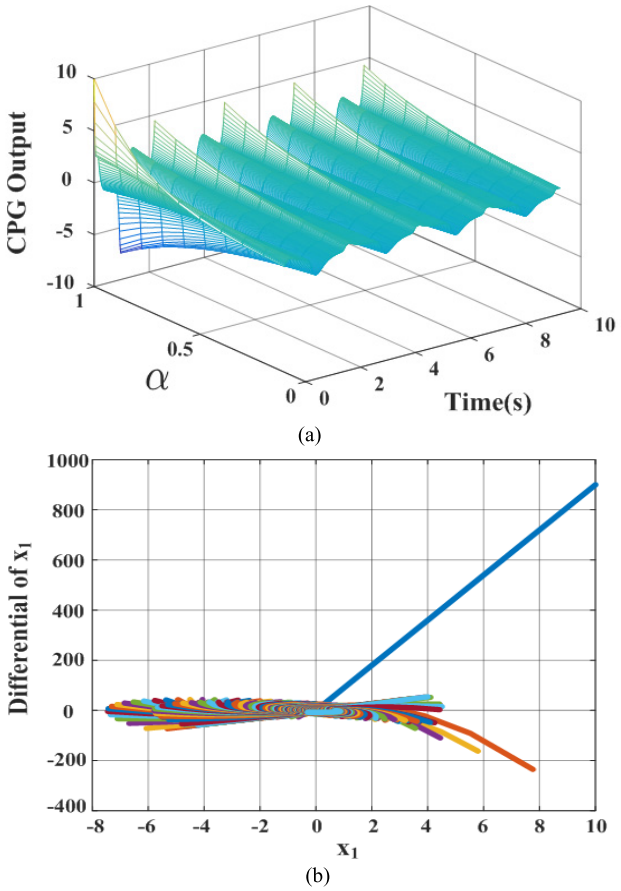

FIGURE 1. Fractional derivatives of CPG output and the phase diagram with order between 0.1 and 1. (a) Fractional derivatives of CPG output. (b) Phase diagram.

Therefore, the fractional order CPG model is obtained and shown below.

$$\begin{cases} {}^{GL}D^{\alpha}x_1 = (-x_1 - bx_2 - wg(x_3) + c)/T_r \\ {}^{GL}D^{\alpha}x_2 = (-x_2 + g(x_1))/T_a \\ {}^{GL}D^{\alpha}x_3 = (-x_3 - bx_4 - wg(x_1) + c)/T_r \\ {}^{GL}D^{\alpha}x_4 = (-x_4 + g(x_3))/T_a \end{cases} \quad (12)$$

And the output of the model is ${}^{GL}D^{\alpha}(g(x_1) - g(x_2))$. In following simulations, parameters T_r and T_a are set as 0.1 and 1, respectively. Parameters c, b and w are chosen as 1, 2.5 and 2.5, respectively. The order α is selected from range [0.1, 1] (with step 0.1). The fractional derivatives of CPG output and the phase diagram are shown in Figure 1.

In order to investigate the difference between the integral order CPG model and the fractional order one, the CPG output and phase diagram base on typical Matsuoka model are obtained. And their differences are shown in Figure 2.

Figures 2(a)-(b) are the CPG output and phase diagram based on the typical Matsuoka model, respectively. Figures 2(c)-(d), Figures 2(e)-(f) and Figures 2(g)-(h) are the characteristics of the fractional order model whose orders are 0.2, 0.5 and 1, respectively. Although the morphology of output and phase diagram with the integer order and fractional

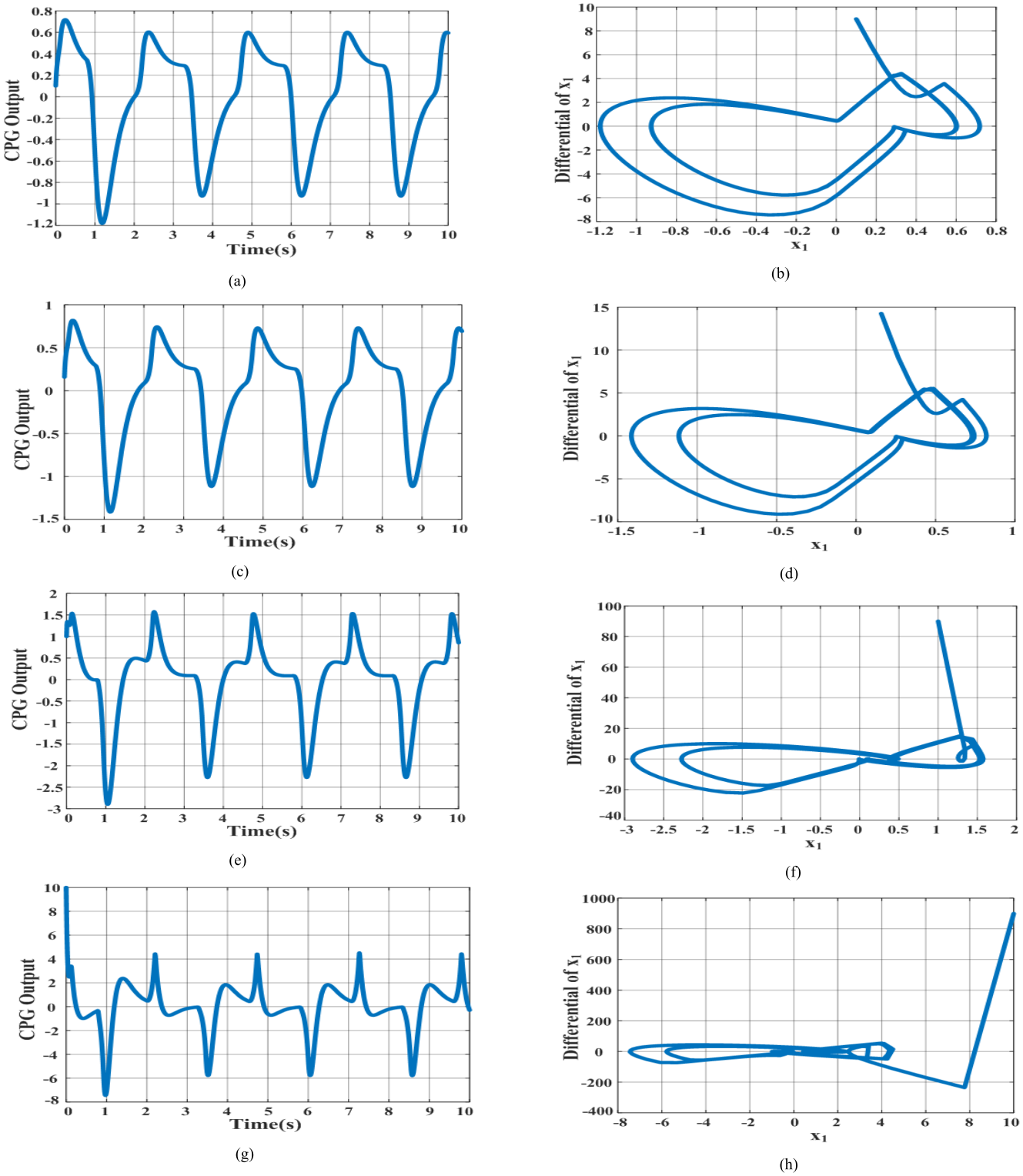

FIGURE 2. Difference between the typical Matsuoka CPG model and the fractional order CPG model. (a) CPG output based on typical Matsuoka model. (b) Phase diagram based on typical Matsuoka model. (c) CPG output with order 0.2. (d) Phase diagram with order 0.2. (e) CPG output with order 0.5. (f) Phase diagram with order 0.5. (g) CPG output with order 1. (h) Phase diagram with order 1.

order CPG model are similar, the CPG output obtained with the fractional order is more accurate than the one obtained with the integral order and it is more suitable for limn the biological information. Increasing the fractional order makes the CPG output more accurate. This shows the abundant dynamic characteristics of the fractional order system.

The following second-order differential equation could be employed to describe the neuron populations in the Jansen's model [32].

$$\ddot{y}(t) = Aa_d x(t) - 2a_d \dot{y}(t) - a_d^2 y(t) \tag{13}$$

In the above equation, the maximum value of the postsynaptic potentials is denoted by A while the overall delays due to the synaptic transmission is represented with a_d.

By change of variables, (13) could be rewritten as

$$\begin{cases} \dot{y}(t) = z(t) \\ \dot{z}(t) = Aa_d x(t) - 2a_d z(t) - a_d^2 y(t) \end{cases} \tag{14}$$

If the fractional order CPG output is considered as the input of relation (14), a time delay fractional order CPG model with the following state space equations is obtained.

$$\begin{cases} {}^{GL}D^{\alpha} x_1 = (-x_1 - bx_2 - wg(x_3) + c)/T_r \\ {}^{GL}D^{\alpha} x_2 = (-x_2 + g(x_1))/T_a \\ {}^{GL}D^{\alpha} x_3 = (-x_3 - bx_4 - wg(x_1) + c)/T_r \\ {}^{GL}D^{\alpha} x_4 = (-x_4 + g(x_3))/T_a \\ \dot{x}_5 = x_6 \\ \dot{x}_6 = Aa_d {}^{GL}D^{\alpha}(g(x_1) - g(x_2)) - 2a_d x_6 - a_d^2 x_5 \end{cases} \tag{15}$$

where x_5 and x_6 correspond to y and z in (14), respectively.

B. MODEL BETWEEN FRACTIONAL ORDER CPG AND MOTOR CORTEX

Based on research results [3], the motor cortex should be coupled with the CPG. Based on previous studies [19], the neural population [32]–[34] is chosen to simulate the motor cortex which has a repetitive columnar structure. The NMM models as a population of pyramidal cells and it is very efficient for determining the steady-state behavior of neuronal systems [19], [32]. Because the principle of the NMM is close to the motor cortex structure, the NMM is selected as the motor cortex in following simulations. Now, the model reflecting the coupling between the fractional order CPG and the motor cortex is derived, as shown in Figure 3.

The NMM model and the fractional order CPG are shown in the right and the left side of Figure 3, respectively. In the NMM, a single neural population is modeled by a population of the pyramidal cells receiving inhibitory and excitatory feedback from local neurons and excitatory input from far and near cortex areas with the connectivity constants C_1, C_2, C_3 and C_4. The average pulse density p represents the excitatory input [31]. Considering the time delay, an appropriate function $h_d(t)$ is employed to transform the output of the fractional order CPG to an average postsynaptic membrane potential. Consider that the obtained signal is multiplied by a constant m. Now, the resultant potential is applied to the NMM. Then, an appropriate feedback function $h_d(t)$ and the gain m are employed to transfer the NMM output to the fractional order CPG block.

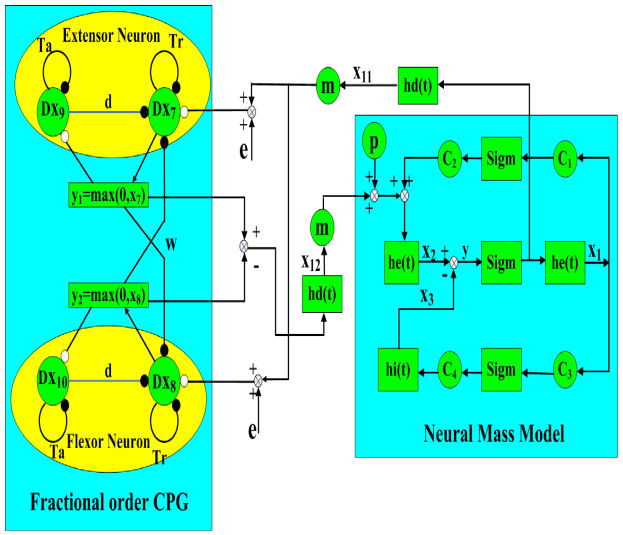

FIGURE 3. Model between motor cortex and fractional order CPG.

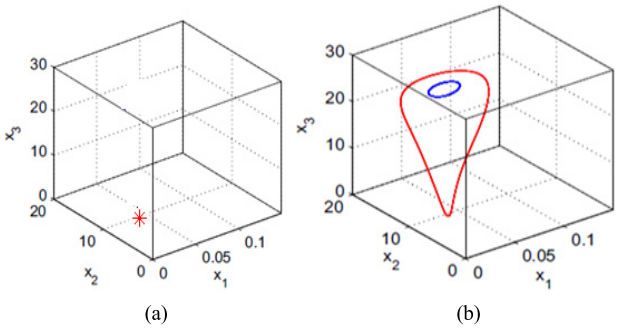

FIGURE 4. Equilibrium points of NMM. (a) The first mode of NMM. (b) The second and the third modes of NMM.

In Figure 3, the impulse response function of time delay $h_d(t)$ [19], [31] is given by.

$$h_d(t) = \begin{cases} Aa_d t e^{-a_d t} (t \geq 0) \\ 0 (t < 0) \end{cases} \tag{16}$$

where A and a_d have the same meaning of ones in (13). If the input is $x(t)$, then the output is $y(t) = h_d * x(t)$.

The state space equations of the overall model could be obtained by combining the state space equations of the fractional order CPG and NMM. Relation (17) gives the obtained equations. Consider that the output of NMM $(x_2 - x_3)$ is connected to the input of the fractional order CPG while the CPG output $(g(x_7) - g(x_8))$ is transferred through a time delay to the NMM input. By dividing the time delay of the excitatory impulse response obtained from the local neurons to k, the parameter $a_d = a/k$ is obtained which is given in (16). These parameters are adjusted [32] for simulation of the relationship between the prefrontal and occipital visual cortex. A constant parameter m is employed for attenuating the one area output before transferring it to the other one through a feedback. These two parameters are

considered as 1.

$$\begin{cases} \dot{x}_1 = x_4 \\ \dot{x}_2 = x_5 \\ \dot{x}_3 = x_6 \\ \dot{x}_4 = AaSigm(x_2 - x_3) - 2ax_4 - a^2 x_1 \\ \dot{x}_5 = AaC_2 Sigm(C_1 x_1) - 2ax_5 - a^2 x_2 + Aa(p + mx_{12}) \\ \dot{x}_6 = BdC_4 Sigm(C_3 x_1) - 2dx_6 - d^2 x_3 \\ {}^{GL}D^{\alpha} x_7 = (-x_7 - bx_9 - wg(x_8) + c + mx_{11})/T_r \\ {}^{GL}D^{\alpha} x_8 = (-x_8 - bx_{10} - wg(x_7) + c + mx_{11})/T_r \\ {}^{GL}D^{\alpha} x_9 = (-x_9 - g(x_7))/T_a \\ {}^{GL}D^{\alpha} x_{10} = (-x_{10} + g(x_8))/T_a \\ \dot{x}_{11} = x_{13} \\ \dot{x}_{12} = x_{14} \\ \dot{x}_{13} = Aa_d Sigm(x_2 - x_3) - 2a_d x_{13} - a_d^2 x_{11} \\ \dot{x}_{14} = Aa_d {}^{GL}D^{\alpha}[g(x_7) - g(x_8)] - 2a_d x_{14} - a_d^2 x_{12} \end{cases} \quad (17)$$

In (17), the maximum rate of firing for the neural population is denoted by $Sigm(v) = 2e_0/(1 + e^{r(v_0 - v)})$. e_0 determines the maximum firing rate of the neural population. The required postsynaptic potential to reach 50% firing rate and the sigmoidal transformation steepness are denoted by v_0 and r, respectively [32]. The corresponding outputs of three postsynaptic potential blocks are indicated by x_1, x_2, and x_3, respectively. The maximum amplitude of the excitatory and inhibitory postsynaptic potentials are denoted by A and B, respectively. The reciprocal summation of the time constants of the passive membrane and other spatially distributed delays in the dendritic network gives a and d. The outputs of the NMM and the time delay fractional order CPG are indicated with x_{11} and x_{12}, respectively.

III. RESULTS

In this section, the connection between the NMM and the fractional order CPG is discussed from two perspectives. At first, the effects of changing parameters p and m on the NMM and the fractional order CPG are investigated. Then, the effects of changing parameters b, c, w and the fractional order on the output of these models are studied.

A. EFFECTS OF PARAMETERS P AND M ON THE FRACTIONAL ORDER CPG AND NMM

The default values for the parameters are considered as $A = 3.25mV$, $a = 100s^{-1}$, $B = 22mV$, $d = 50s^{-1}$, $r = 0.56mV$, $e_0 = 2.5s^{-1}$, $v_0 = 6mV$, $C_1 = 1.25C_2 = 4C_3 = 4C_4 = C = 135$ [19], [31], [32]. Changing parameter p leads to different equilibrium points which are shown in Figure 4.

The first mode of the NMM or its equilibrium point is indicated with the red star in Figure 4(a) while its second mode or the spike-like epileptic activity is indicated with a red cycle in Figure 4(b). The third mode or the alpha-like activity is described with the blue cycle in Figure 4(b).

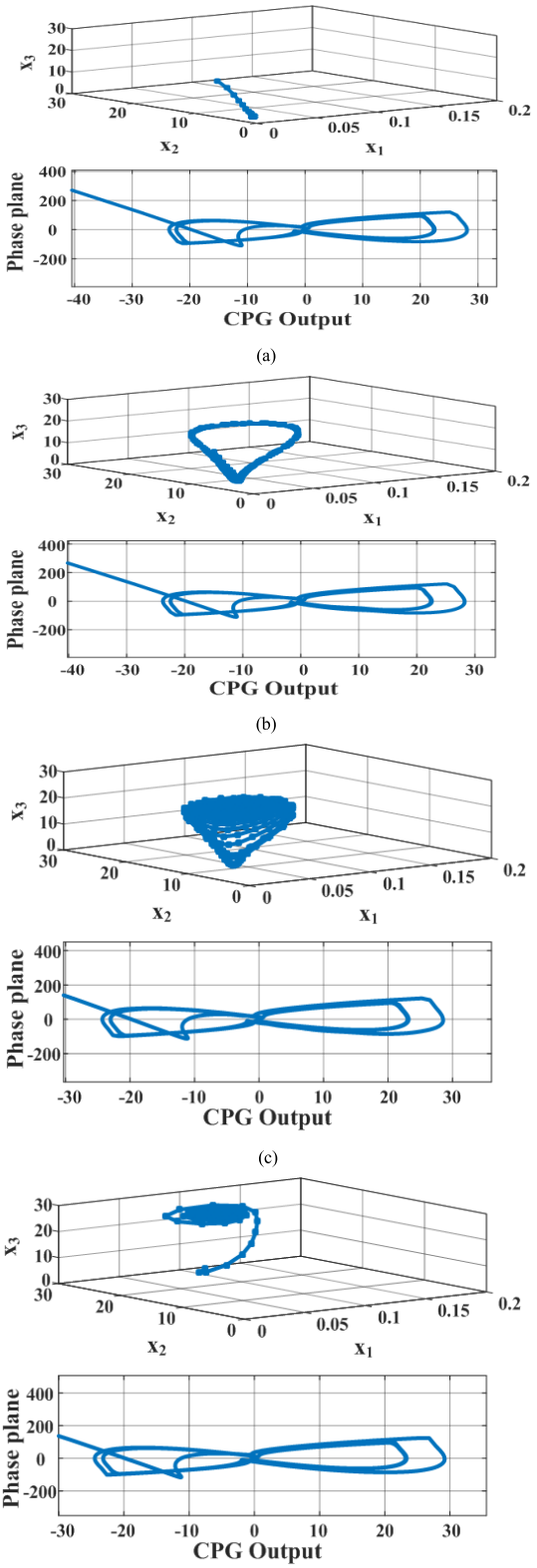

FIGURE 5. State trajectories of the models. (a) $p = 10$. (b) $p = 113$. (c) $p = 139$. (d) $p = 361$.

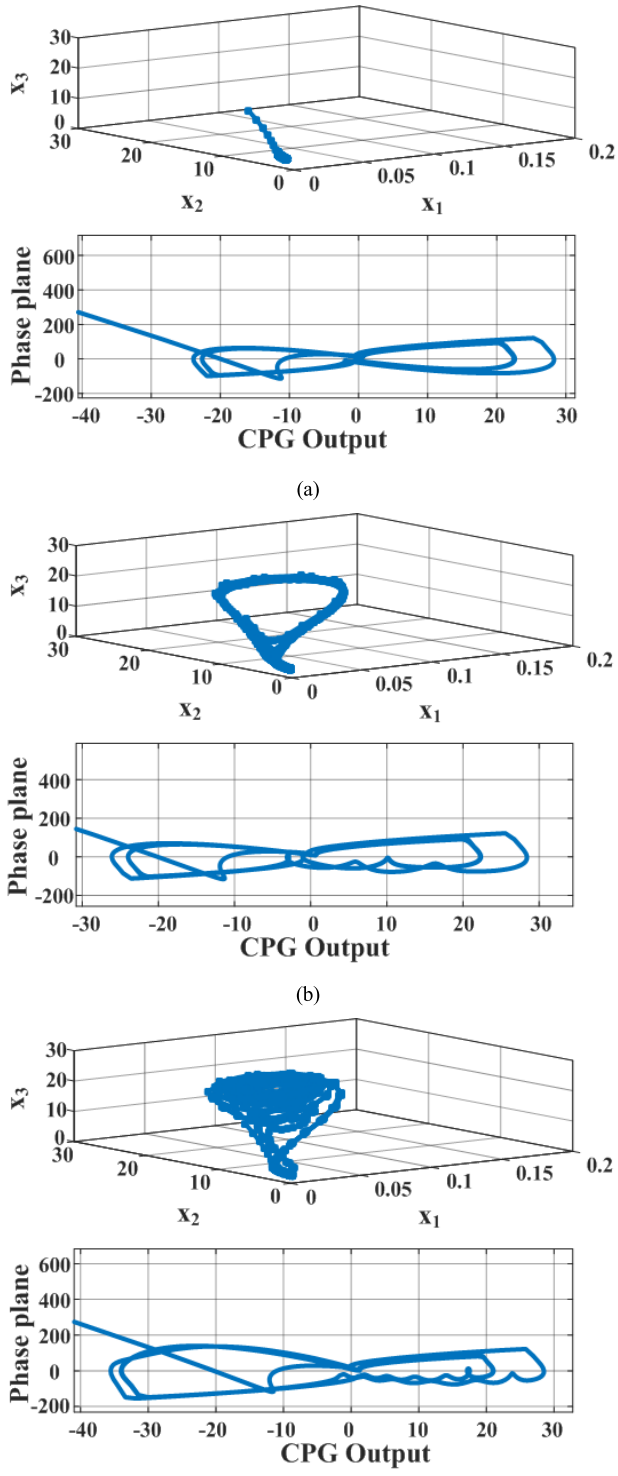

FIGURE 6. State trajectories of the models with $p = 62$. (a) $m = 5$. (b) $m = 12$. (c) $m = 31$.

The remaining parameters are considered as $T_r = 0.1$, $T_a = 1$, $b = 1.6$, $c = 10$, $w = 1.1$, $m = 1$ and $k = 3$ [5], [19] and the order of the fractional order CPG is 0.5.

The NMM modes could vary in accordance with variations of the parameter p [31]. Figure 5 shows how the state

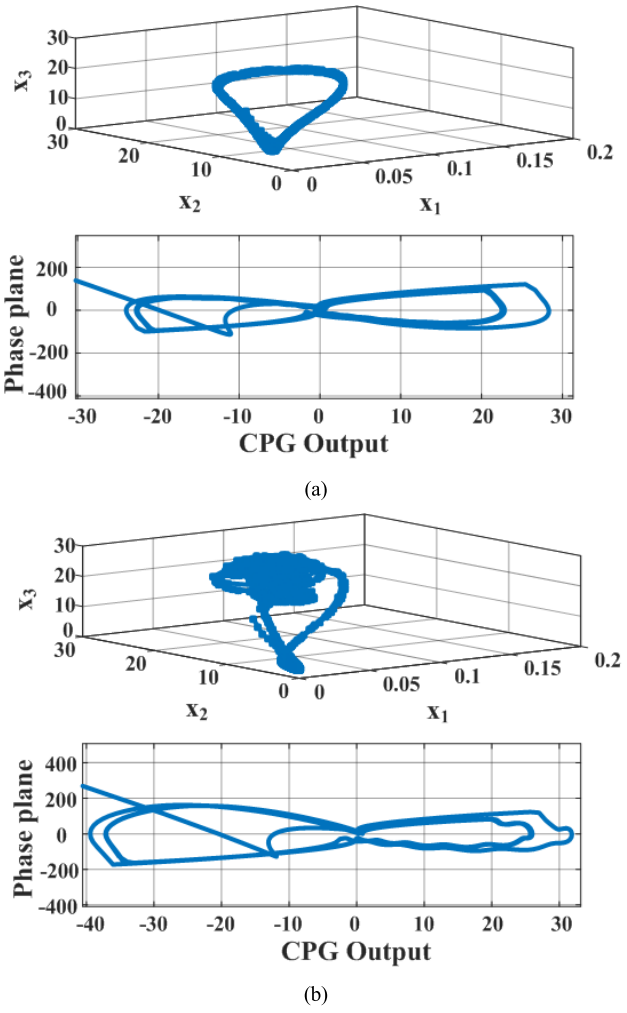

FIGURE 7. State trajectories of the models with $p = 127$. (a) $m = 1$. (b) $m = 17$.

trajectories of the NMM and the fractional order CPG are varied with changing the parameter p.

If $p \in [0, 61]$, the first mode of the NMM could be observed. As could be seen in Figure 5(a), if $p = 10$, periodic oscillations are observed in the fractional order CPG output or equivalently a limit cycle is generated in its state trajectory. Considering $p = 113$ leads to switch from the first mode to the second one (Figure 5(b)). Figure 5(c) shows that further increasing of p (e.g., $p = 139$) causes to switch from the second mode to the third one. According to Figure 5(d), if p exceeds 161, the second and third modes are merged to the third one. Therefore, parameter p has the same function which leads to the switch of the NMM states.

Now, let to verify the impact of parameter m on state trajectories of the fractional order CPG and the NMM. Firstly, the first mode is discussed. Parameter p is considered as 62. If $m = 5$, only the first mode is observed in the NMM and an oscillatory output is obtained for the fractional order CPG (Figure 6(a)). If m exceeds 10, the second mode is generated.

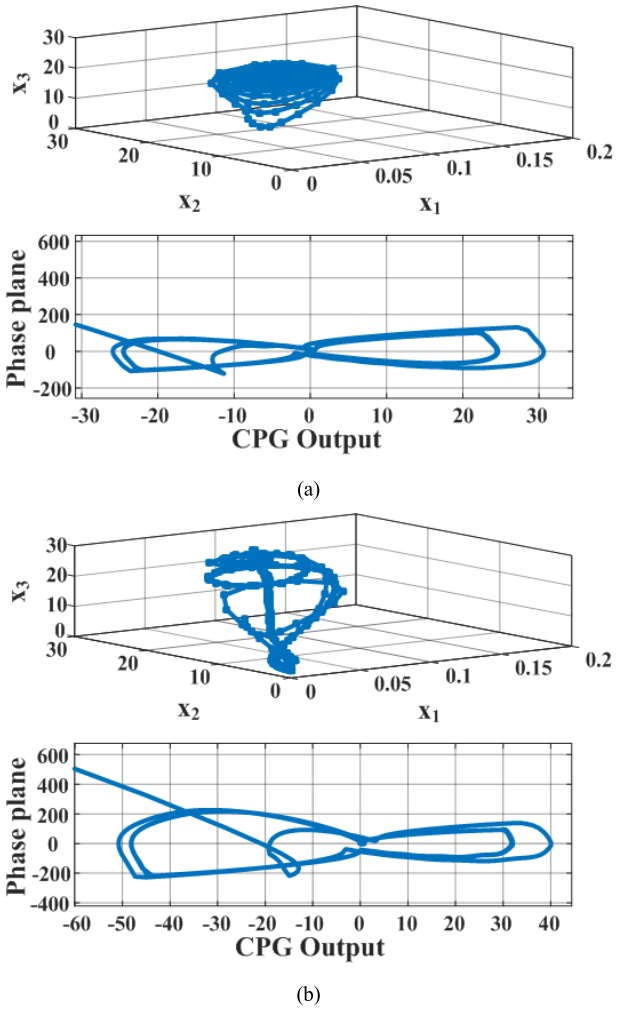

FIGURE 8. State trajectories of the models with $p = 175$. (a) $m = 3$. (b) $m = 26$.

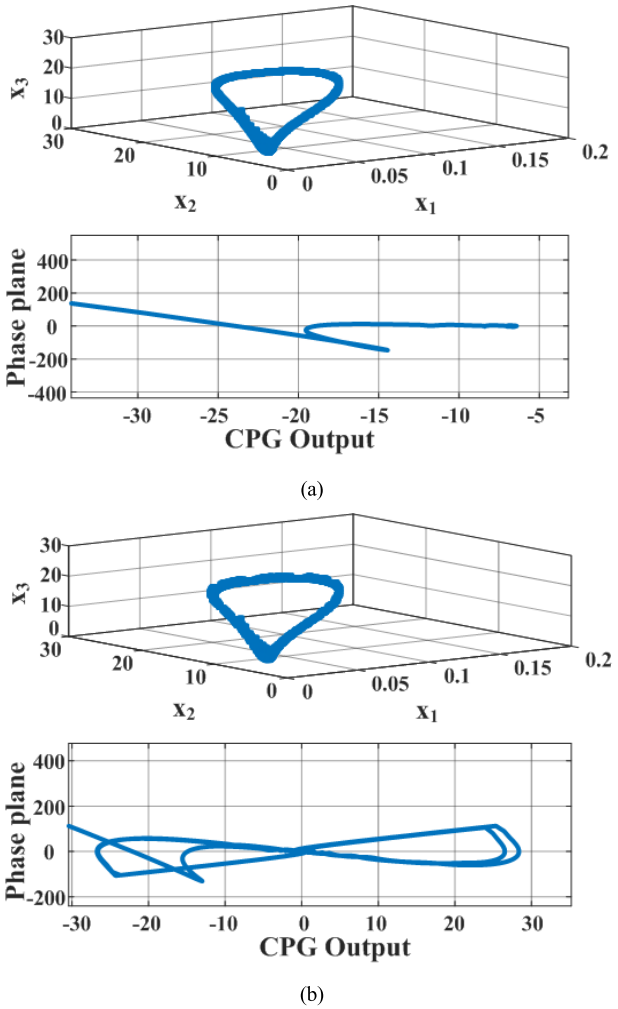

FIGURE 9. State trajectories of the models with the parameter b and $p = 127$. (a) $b = 0$. (b) $b = 0.7$.

The state trajectories obtained for $m = 12$ confirms this fact (Figure 6(b)). Further increasing of parameter m leads to the merging of the second and the third modes (Figure 6(c) for $m = 31$).

Now, let to discuss about the second case for $p = 127$. For $m = 1$, the second mode is appeared in the NMM. This produces a limit cycle in state trajectories of the fractional order CPG (Figure 7(a)). Both the second and the third modes could be appeared by increasing parameter m. When $m = 17$, the second and the third modes merge together (Figure 7(b)).

Now, consider $p = 175$ for the third case. For $m = 3$, both the second and third modes are appeared in the NMM while the significant mode is the third one. This generates a limit cycle that could be seen in the state trajectory of the fractional order CPG (Figure 8(a)). As parameter m increases, the second and the third modes merge. For example, see the results obtained for $m = 26$ in Figure 8(b).

In the three cases mentioned above, the CPG mode is the limit cycle and the NMM starts with its first corresponding mode. By increasing parameter m, the second and the third modes will be appeared independently. When parameter m is larger than a threshold value, the second and the third modes merge together. During this procedure, the NMM is stable while a limit cycle could be seen in the state trajectory of the CPG. Therefore, changing parameter m while maintaining p unchanged leads to conversion of the NMM and the fractional order CPG states.

B. EFFECTS OF PARAMETERS B, C, W AND THE FRACTIONAL ORDER ON NMM AND THE FRACTIONAL ORDER CPG

To investigate how the NMM and the CPG are affected by parameters b, c, w and the fractional order, p is chosen as 127 that is compatible with the second mode of the NMM. At first, if b is equal to zero, the output of the fractional order CPG tends to zero, and the second mode of NMM can be observed (Figure 9(a)). As could be seen from Figure 9(b), increasing parameter b to 0.7 leads to the limit cycle phenomenon in the

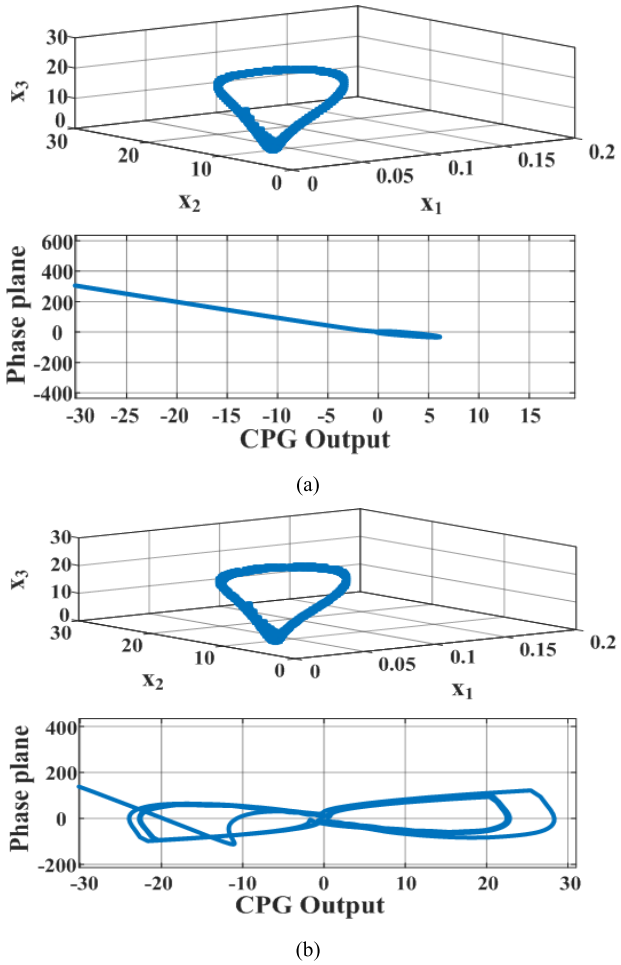

FIGURE 10. State trajectories of the models with the parameter w and $p = 127$. (a) $w = 0.2$. (b) $w = 1.5$.

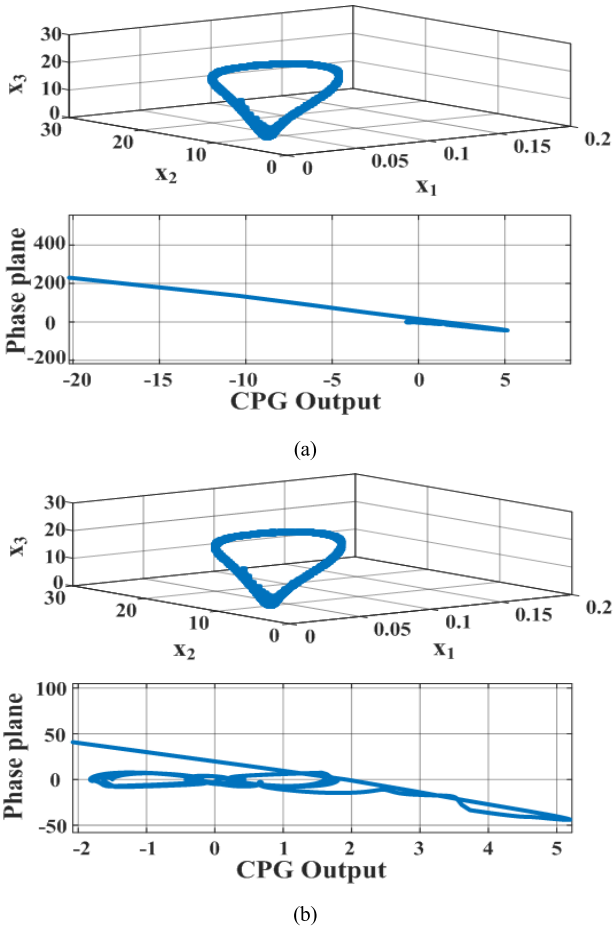

FIGURE 11. State trajectories of the models with the parameter c and $p = 127$. (a) $c = 0.2$. (b) $c = 0.7$.

state trajectory of the CPG. If b exceeds 21, the state trajectory of the CPG tends to the zero plane.

Now, let to verify the effect of changing parameter w. For $w = 0.2$, the second mode of the NMM is generated and the output of the fractional order CPG converges to zero (Figure 10(a)). Figure 10(b) demonstrates that the limit cycle phenomenon occurs in the state trajectory of the fractional order CPG when parameter w is increased to 1.5. Selecting values for w more than 2.7, tends the fractional order CPG output to zero.

In the following, the effect of parameter c is studied. If $c = 0.2$, the NMM falls in its second mode and the output of the fractional order CPG tends to zero (Figure 11(a)). As could be seen from Figure 11(b), the limit cycle is inevitable in the state trajectory of the fractional order CPG when c is increased to 0.7.

The effect of the fractional order on the state trajectories is verified as follows. For $\alpha = 0.1$, the second mode of the NMM is appeared and a limit cycle in the state trajectory combined with an oscillatory output could be obtained (Figure 12(a)). Figure 12(b) shows that closing the fractional order to 1 ($\alpha = 0.7$) leads to considerable variations in the state trajectory of the NMM and the fractional order CPG, and the second mode begins to switch to next state. When $\alpha = 1$, the coexistence of the second and third modes in the NMM is occurred while the dominant mode is the third one, as shown in Figure 12(c).

The above studies demonstrates that the NMM output and the state trajectories of the fractional order CPG change in accordance with changes in parameters b, c, w and α. Parameter b reflects the self-inhibition strength of the CPG model. As parameter b increases, the state trajectory of the CPG gradually closes to the limit cycle. When b is increased, the state trajectory of the fractional order CPG tends to the zero plane owing to the strong inhibitory effect. The inhibition strength among CPGs could be represented with parameter w. If this parameter is selected from an appropriate range, the CPG output becomes oscillatory and the NMM system becomes stable. The excitatory tonic input is depicted in parameter c. The CPG output amplitude depends on this parameter. As parameter c increases, the state trajectory of the CPG gradually switches to the limit cycle. Based on above results, the fractional order of the CPG model leads to switching of the NMM modes.

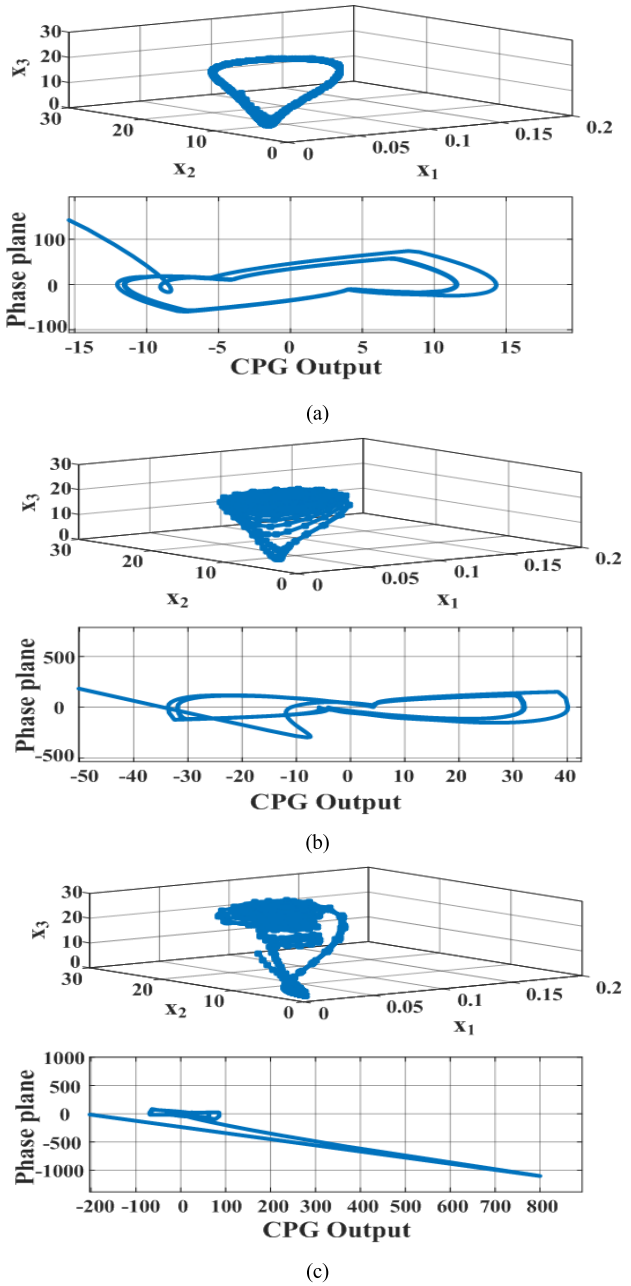

FIGURE 12. State trajectories of the models with the parameter α and $p = 127$. (a) $\alpha = 0.1$. (b) $\alpha = 0.7$.(c) $\alpha = 1$.

IV. CONCLUSION

Comparing with previous studies [19], [27], [28], the proposed model combining the fractional order CPG and the NMM has considerable dynamic characteristics that could help the researchers to derive the relation between the motor cortex and the locomotion. The dynamic properties of this model show that the NMM and the fractional order CPG states could be formed by adjusting its parameters. This means that the locomotor patterns could be controlled via the motor cortex by appropriate adjustment of these variables. Stable locomotion patterns could be formed by interaction between the motor cortex, body segments, and the environment. Different CPG state responses could be obtained by choosing different values for these parameters. Choosing specific values for these parameters leads to the limit cycle in the state trajectory of the fractional order CPG model and stable states for the NMM model.

Unlike the integer order coupling model [19], some new phenomena could be obtained by the fractional order one. First of all, the third mode of the NMM does not exist independently due to the input of the fractional order CPG. Two different outputs are observed. The common property of the two outputs is the coexistence of the second mode and the third mode. The differences are their output patterns in which one is independent and the other is mergence. The second is the effects on the NMM when the parameters b , c and w of the fractional order CPG model are varied. In the integral order model [19], the modes of NMM could switch when the parameters of CPG are altered. However, the modes of NMM cannot change and only the output alters in the fractional order model. The third is the effects on the NMM mode when the fractional order is varied. With the increase of the fractional order, the NMM mode changes from the first mode, the second mode, the coexistence of the second and the third modes and the converge state. Therefore, the fractional order has the same function on the NMM as the parameter p in NMM. With the introduction of the fractional order model, a stable state emerges and can be used to explain the emergence of the new motor mode based on the existing modes. Therefore, the simulation results not only confirm the corresponding relation between the motor cortex and the CPG, but also provide an innovative method which is the introduction of the fractional calculus to produce the new locomotion state.

In order to apply the coupling model to robot control, it is a worthy field in which the researchers realize the nonlinear networks and their working mechanism. Researchers [35] have attempted to apply the field programmable gate array (FPGA) to biology and neuroscience. The investigations show that FPGA is more effective than software in neural network. At the same time, the researchers also develop the silicon chip to describe the biological CPG [36]. Therefore, it is deserved to further study how to design a chip which shows the structure of the neural network and the CPG.

REFERENCES

[1] J. Yu, M. Tan, J. Chen, and J. Zhang, "A survey on CPG-inspired control models and system implementation," *IEEE Trans. Neural Netw. Learn. Syst.*, vol. 25, no. 3, pp. 441–456, Mar. 2014.

[2] L. Minati, M. Frasca, N. Yoshimura, and Y. Koike, "Versatile locomotion control of a hexapod robot using a hierarchical network of nonlinear oscillator circuits," *IEEE Access*, vol. 6, no. 99, pp. 8042–8065, Jan. 2018.

[3] S. Grillner, "Human locomotor circuits conform," *Neuroscience*, vol. 334, no. 6058, pp. 912–913, Nov. 2011.

[4] K. Matsuoka, "Sustained oscillations generated by mutually inhibiting neurons with adaptation," *Biol. Cybern.*, vol. 52, no. 6, pp. 367–376, Oct. 1985.

[5] K. Matsuoka, "Analysis of a neural oscillator," *Biol. Cybern.*, vol. 104, pp. 297–304, May 2011.

[6] S. Campbell and D. Wang, "Synchronization and desynchronization in a network of locally coupled Wilson-Cowan oscillators," *IEEE Trans. Neural Netw.*, vol. 7, no. 3, pp. 541–554, May 1996.

[7] Y. Song, J. Wei, and Y. Yuan, "Stability switches and Hopf bifurcations in a pair of delay-coupled oscillators," *J. Nonlinear Sci.*, vol. 17, no. 2, pp. 145–166, Apr. 2007.
[8] C. A. K. Kwuimy and B. R. N. Nbendjo, "Active control of horseshoes chaos in a driven Rayleigh oscillator with fractional order deflection," *Phys. Lett. A*, vol. 375, no. 39, pp. 3442–3449, Sep. 2011.
[9] L. Lin, L. Zheng, Y. Chen, and F. Liu, "Anomalous diffusion in comb model with fractional dual-phase-lag constitutive relation," *Comput. Math. Appl.*, vol. 76, no. 2, pp. 245–256, Jul. 2018.
[10] R. L. Magin, "Fractional calculus models of complex dynamics in biological tissues," *Comput. Math. Appl.*, vol. 59, no. 5, pp. 1586–1593, 2010.
[11] K. Moaddy, A. G. Radwan, K. N. Salama, S. Momani, and I. Hashim, "The fractional-order modeling and synchronization of electrically coupled neuron systems," *Comput. Math. Appl.*, vol. 64, no. 10, pp. 3329–3339, 2012.
[12] S. H. Weinberg, "Membrane capacitive memory alters spiking in neurons described by the fractional-order hodgkin-huxley model," *PLoS ONE*, vol. 10, no. 5, May 2015, Art. no. e0126629.
[13] W. W. Teka, R. K. Upadhyay, and A. Mondal, "Fractional-order leaky integrate- and-fire model with long-term memory and power law dynamics," *Neural Netw.*, vol. 93, pp. 110–125, Sep. 2017.
[14] N. C. Ha and K. J. Dougherty, "Spinal shox2 interneuron interconnectivity related to function and development," *Neuron*, vol. 7, Art. no. e42519, Dec. 2018.
[15] R. M. Brownstone and J. M. Wilson, "Strategies for delineating spinal locomotor rhythm-generating networks and the possible role of Hb9 interneurones in rhythmogenesis," *Brain Res. Rev.*, vol. 57, no. 1, pp. 64–76, Jan. 2008.
[16] O. Kiehn, "Locomotor circuits in the mammalian spinal cord," *Annu. Rev. Neurosci.*, vol. 29, pp. 279–306, Jul. 2006.
[17] M. Hägglund, K. J. Dougherty, L. Borgius, S. Itohara, T. Iwasato, and O. Kiehn, "Optogenetic dissection reveals multiple rhythmogenic modules underlying locomotion," *Proc. Nat. Acad. Sci. USA*, vol. 110, no. 28, pp. 11589–11594, Jul. 2013.
[18] G. Zhong, L. Chen, Z. Jiao, J. Li, and H. Deng, "Locomotion control and gait planning of a novel hexapod robot using biomimetic neurons," *IEEE Trans. Control Syst. Technol.*, vol. 26, no. 2, pp. 624–636, Mar. 2018.
[19] Q. Lu, "Coupling relationship between the central pattern generator and the cerebral cortex with time delay," *Cogn. Neurodyn.*, vol. 9, no. 4, pp. 423–436, Aug. 2015.
[20] O. Kiehn, "Decoding the organization of spinal circuits that control locomotion," *Nature Rev. Neurosci.*, vol. 17, pp. 224–238, Mar. 2016.
[21] A. Roberts, W.-C. Li, and S. R. Soffe, "A functional scaffold of CNS neurons for the vertebrates: The developing xenopus laevis spinal cord," *Develop. Neurobiol.*, vol. 72, no. 4, pp. 575–584, Apr. 2012.
[22] N. Dominici *et al.*, "Locomotor primitives in newborn babies and their development," *Science*, vol. 334, no. 6058, pp. 997–999, Nov. 2011.
[23] H. J. Chiel, L. H. Ting, O. Ekeberg, and M. J. Hartmann, "The brain in its body: Motor control and sensing in a biomechanical context," *J. Neurosci.*, vol. 29, no. 41, pp. 12807–12814, 2009.
[24] F. Lacquaniti, Y. P. Ivanenko, and M. Zago, "Patterned control of human locomotion," *J. Physiol.*, vol. 590, no. 10, pp. 2189–2199, May 2012.
[25] A. C. Murphy *et al.*, "Structure, function, and control of the human musculoskeletal network," *PLoS Biol.*, vol. 16, no. 1, Dec. 2016, Art. no. e2002811.
[26] J. N. Kerkman, A. Daffertshofer, L. L. Gollo, M. Breakspear, and T. W. Boonstra, "Network structure of the human musculoskeletal system shapes neural interactions on multiple time scales," *Sci. Adv.*, vol. 4, no. 6, Jun. 2018, Art. no. eaat0497.
[27] Q. Lu and J. Tian, "Synchronization and stochastic resonance of the small-world neural network based on the CPG," *Cogn. Neurodyn.*, vol. 8, no. 3, pp. 217–226, Jun. 2014.
[28] Q. Lu, W. Li, J. Tian, and X. Zhang, "Effects on hypothalamus when CPG is fed back to basal ganglia based on KIV model," *Cogn. Neurodyn.*, vol. 9, no. 1, pp. 85–92, Feb. 2015.
[29] A. M. A. El-Sayed, A. E. M. El-Mesiry, and H. A. A. El-Saka, "On the fractional-order logistic equation," *Appl. Math. Lett.*, vol. 20, no. 7, pp. 817–823, Jul. 2011.
[30] W. Deng, C. Li, and J. Lü, "Stability analysis of linear fractional differential system with multiple time delays," *Nonlinear Dyn.*, vol. 48, no. 4, pp. 409–416, 2007.
[31] G. Huang, D. Zhang, J. Meng, and X. Zhu "Interactions between two neural populations: A mechanism of chaos and oscillation in neural mass model," *Neurocomputing*, vol. 74, no. 6, pp. 1026–1034, Feb. 2011.
[32] B. H. Jansen and V. G. Rit, "Electroencephalogram and visual evoked potential generation in a mathematical model of coupled cortical columns," *Biol. Cybern.*, vol. 73, no. 4, pp. 357–366, Sep. 1995.
[33] F. Grimbert and O. Faugeras, "Bifurcation analysis of Jansen's neural mass model," *Neural Comput.*, vol. 18, no. 12, pp. 3052–3068, Dec. 2006.
[34] E. J. Nichols and A. Hutt, "Neural field simulator: Two-dimensional spatio-temporal dynamics involving finite transmission speed," *Frontiers Neuroinform.*, vol. 9, p. 25, Oct. 2015.
[35] B. Deng, Z. Zhu, S. Yang, X. Wei, J. Wang, and H. Yu, "FPGA implementation of motifs-based neuronal network and synchronization analysis," *Phys. A, Stat. Mech. Appl.*, vol. 451, pp. 388–402, Jun. 2016.
[36] A. Aggarwal, "VLSI realisation of neural velocity integrator and central pattern generator," *Electron. Lett.*, vol. 51, no. 18, pp. 1405–1407, Aug. 2015.

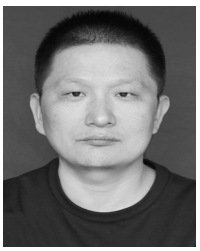

QIANG LU was born in Tai'an, Shandong, China, in 1975. He received the B.S. degree from the Qingdao University of Science and Technology, Qingdao, China, the master's degree from the Shandong University of Science and Technology, Qingdao, and the Ph.D. degree in control theory and control engineering from Tongji University, Shanghai, China.

He is currently an Association Professor with the College of Medical Information Engineering, Shandong First Medical University & Shandong Academy of Medical Sciences, Tai'an. His current research interests include neural computation, intelligent robot control, and nonlinear dynamics.